Investigation of Ether-Based Ionic Liquid Electrolytes for Lithium-O_2 Batteries

S. Ferrari,[ab*] E. Quartarone,[b] C. Tomasi,[bc] M. Bini,[b] P. Galinetto,[d] M. Fagnoni,[b] P. Mustarelli[b]

[a] WMG, University of Warwick, Gibbet Hill Road, CV4 7AL Coventry, UK

[b] Dep. of Chemistry, University of Pavia, Via Taramelli 16, 27100 Pavia, Italy

[c] I.E.N.I. C.N.R. U.O.S. of Lecco, C.so Promessi Sposi 29, 23900 Lecco, Italy

[d] Dep. of Physics, University of Pavia, Via Bassi 6, 27100 Pavia, Italy

*Corresponding Author: S.Ferrari@warwick.ac.uk

Abstract

In this work, we showed the results of the characterization of ether based electrolytes for Li-O_2 batteries, prepared by mixing TEGDME and *N*-methoxyethyl-*N*-methylpyrrolidinium bis(trifluoromethanesulfonyl)-imide ionic liquid (IL). The mixtures having different ratio TEGDME/IL and containing $LiCF_3SO_3$ salt, were thoroughly characterized by thermal analysis, conductivity and electrochemical stability measurements. Their potential use as electrolytes in Li-O_2 batteries was checked investigating Li/TEGDME-IL/O_2 cells by means of cycling voltammetry (CV) and galvanostatic charge-discharge tests.

Keywords: electrochemistry, ionic liquids, Li-air batteries, cyclic voltammetry, Raman spectroscopy

1. Introduction

Li-air batteries (LABs) are nowadays under intense study due to their promise of energy storage that could meet, although in the long term, the demands of expanding markets, such as automotive and stationary storage for smart grids.[1-2] In principle, the reaction mechanism is very simple and involves Li ions and O_2 to form Li_2O_2. However, problems related with the chemistry and electrochemistry of LABs are severe, and extensive efforts are required to address them, in order to make these batteries a commercial viable successor to Li-ion batteries (LIBs).[3-4] Among the possible cells, the aprotic one based on the use of organic solvents as the electrolyte has attracted a lot of interest because these solvents can circumvent lithium corrosion and restrict safety issues due to possible H_2 formation with aqueous electrolytes.[5-6] The identification of stable solvents for aprotic rechargeable LABs is undoubtedly one of the major challenges to face for the successful development of this technology.[6-7]A variety of electrolytes were tested so far, starting from organic carbonates such as EC, PC, DEC etc., which were soon discarded due to their rapid decomposition during discharge.[5, 8-9] Then esters,[10] nitriles,[11] amides[12-13] and DMSO-based electrolytes[14-15] were proposed, but none of these seems to have all the necessary requirements for the application in LABs, which include high oxygen solubility, low reactivity at the Li metal anode, stability towards nucleophilic attack by oxygen reduction species, low flammability, low vapour pressure to prevent huge electrolyte loss, and high ionic conductivity.[5] Ethers and glymes are instead considered as promising candidates for the aprotic Li-air battery[16-18] due to their good stability against nucleophilic attack, even if for prolonged cycling together with Li_2O_2 as the main reaction product, a mixture of Li_2CO_3, HCO_2Li, CH_3CO_2Li and other decomposition products were identified in the cathode.[8,19] Also ionic liquids (ILs) are under intense investigation,[20] since some of their properties are fully within the requirements of LAB electrolytes, but the research in this field is still at an early stage. One of the main drawbacks of ILs is a low Li^+ transference number that still hinders their huge application in Li batteries. However, the potential of ILs not only as electrolytes,[21-27] but also as solvents to prepare gel cathodes, deserves to be studied at the light of recent results.[28-29] The implementation of blended electrolytes was recently proposed with

the aim of overcoming components drawbacks, combining the useful properties of each components,[5] and the mixtures of tetraethylene glycol dimethyl ether (TEGDME) and $PYR_{14}TFSI$,[30] or PC and $PYR_{13}TFSI$,[31] demonstrated good conductivity and electrolyte stability.

In this paper, we try to combine useful electrolyte features by blending TEGDME and *N*-methoxyethyl-*N*-methylpyrrolidinium bis(trifluoromethanesulfonyl)-imide ionic liquid ($PYR_{1,2O1}TFSI$).[32] Different compositions in volume were characterized from the chemical-physical point of view and specifically, oxygen reduction (ORR) and evolution (OER) reactions have been studied in order to obtain information on the reversibility of the electrochemical process.

2. Experimental

2.1 Electrolytes preparation

$PYR_{1,2O1}TFSI$ was synthesised according to the procedure reported in ref. [32]. TEGDME (≥99%) was obtained from Sigma Aldrich and used as received. The volume ratio between the IL and TEGDME was $xPYR_{1,2O1}$:(1-x)TEGDME V/V % with x=0, 30, 50, 70. Lithium trifluoromethanesulfonate (Lithium triflate, LiTf battery grade, Ferro Corp.) was chosen as salt because of its slightly superior stability on cycling and lower charge voltage plateau than the LiTFSI one. LiTf was dissolved in the blended solvents to obtain a final concentration of 0.5M. All the mixtures were prepared in a dry box (H_2O, O_2< 1 ppm) under argon atmosphere.

2.2 Characterization

Differential Scanning Calorimetry (DSC) measurements were performed with a 2910 MDSC (TA Instruments), at a rate of 5°Cmin^{-1} under nitrogen purge by using either standard or hermetic aluminium pans depending on the analysed sample. Thermogravimetric analysis (TGA) measurements were carried out at 5°Cmin^{-1} under N_2 purge in a 2950 TGA (TA Instruments), up to 600°C.

The ionic conductivity was measured by means of the impedance spectroscopy technique, using a frequency response analyser (FRA Solartron 1255), connected to an electrochemical interface (Solartron 1287), over the frequency range 1 Hz-1 MHz, by applying a voltage of 50 mV. The impedance scans were carried out in the temperature range -25°C and 80°C, by using a cell for liquids with two platinum electrodes (cell constant of 0.35 cm^{-1}).

In order to study the electrolyte stability vs Li, potentiodynamic sweeps were performed by means of an Autolab potentiostat PGSTAT30 (Eco Chemie). The three-electrodes gas tight cell was made of glassy carbon as the working electrode, a Pt wire as the counter one and Ag/Ag^+ (CH_3CN, 1 mM $AgNO_3$) as the reference. The reference electrode was calibrated vs Fc/Fc^+ redox couple and the effective electrode area of the glassy carbon electrode, 0.033 cm^2, was calculated from cyclic voltammograms on a 1 mM ferrocene solution in CH_3CN (0.1M tetrabutylammonium perchlorate), by applying the Randles-Sevcik equation to the resulting peak current:

$$ip=0.4463nF(nF/RT)^{1/2}AD^{1/2}v^{1/2}c \quad (1)$$

where i_p is the peak current, n is the number of electrons in the charge transfer step, A is the electrode area, D is the diffusion coefficient of Fc ($2.3\ 10^{-5} cm^2\ s^{-1}$)[33] c is the concentration and v the scan rate ($10\ mVs^{-1}$).

2.3 Air cathode preparation, cell assembly and tests

Carbon material (Vulcan XC72R, 80%) and polyvinylidene fluoride binder (PVDF Solvay, 20%) were mixed in an N-methyl-2-pyrrolidone (NMP, Sigma Aldrich) solution and the resulting slurry was coated on a gas diffusion layer (Toray TGP-H-060).

Swagelok-type, three-electrodes cells were assembled in the dry-box under argon atmosphere by using lithium as anode and reference electrode, Whatman discs as separators and the abovementioned carbon cathode. The plunger facing the carbon cathode had been bored hollow,[28] in order to allow oxygen to flow inside the carbon cathode (0.02 L/h). The cell was investigated by CV using an

Autolab potentiostat PGSTAT30 (Eco Chemie) at a scan rate of 0.1 $mVsec^{-1}$ in the 2.4-4.2V potential range.

For galvanostatic charge-discharge tests an ECC-Air electrochemical cell (EL-Cell) was assembled; a lithium disc was used as the anode and a Whatman GF/A was used as separator. The separator was saturated with the electrolyte mixtures. The cells were cycled by using an Arbin BT-2000 battery cycler at room temperature in the 2.2-3.9V potential range at current densities 10-40 mAg_{carbon}^{-1}.

Scanning Electron Microscopy (SEM) micrographs of the discharged carbon cathode surface were acquired by using a Zeiss EVO®-MA10-HR microscope.

Micro-Raman measurements were carried out at room temperature by using a Labram Dilor spectrometer equipped with an Olympus microscope HS BX40. The 632.8 nm light from He-Ne laser was employed as excitation radiation and it was focused with a 50x objective obtaining a laser spot of ~0.7 μm of diameter. The spectral resolution was about 1 cm^{-1}. In order to avoid any possible reactive effect the samples were kept in pure nitrogen using an atmosphere-controlled optical cell.

3. Results and discussion

3.1 Thermal stability

The quite high thermal stability of the $PYR_{1,2O1}$TFSI ionic liquid was discussed in a previous work[32] and is herein confirmed (see Figure 1). Conversely, the decomposition of TEGDME starts at temperatures as low as 110°C and its mass residue is practically negligible already at 200°C, thus indicating the completion of the breakdown process. The 0.5M LiTf mixture shows a decomposition temperature just slightly higher than that of pristine TEGDME, due to presence of salt. As expected, for what concerns the $xPYR_{1,2O1}(1-x)$TEGDME mixtures, the weight loss shows two clear main steps. The first loss at lower temperatures is due to TEGDME decomposition and takes place nearly at the same temperature as the one observed for the 0.5M solution. The second weight loss, falling at higher temperatures (~400 ºC), can be easily ascribed to the IL decomposition. A good correspondence

between mixture composition and the weight step extents can be found, if the amount of residue at the end of each measurement, which is likely due to the inorganic fraction of the salt, is taken into account (see Figure 1a).

The DSC traces recorded on the mixtures are reported in Figure 1b. As shown in a previous work, $PYR_{1,2O1}TFSI$ exhibits a glass transition (T_g) at about -87 °C (DSC trace not reported here) and no further thermal features were detected in the investigated temperature range (up to 300°C).[32] The thermogram of the TEGDME:0.5M LiTf solution shows an almost sharp melting peak at about -32°C, and two broad endotherms above 100°C which are related to the decomposition process. A melting endotherm was observed at -30 ºC for pristine TEGDME (not shown).

All the IL-based mixtures present a T_g at low temperatures, followed by an incipient cold crystallization (more evident for 30:70 and 50:50 mixtures) and decomposition phenomena above 100ºC. For the $30PYR_{1,2O1}$:70TEGDME and $50PYR_{1,2O1}$:50TEGDME compositions the T_g values are somewhat lower than that of pure IL, -96 and -90°C respectively, while for the composition richer in IL, $70PYR_{1,2O1}$:30TEGDME, the T_g falls pretty at the same temperature as for pure IL (within the experimental error). This glass transition temperature trend can be explained by admitting that TEGDME plays as a plasticizer in the mixtures, so that higher amounts of such a solvent lead to more plasticized solutions and, in turn, to lower T_g values. An analogous behaviour was observed by Shin et al. [33] on a similar system in which $PYR_{14}TFSI$ was employed.

3.2 Ionic conductivity and electrochemical stability

Figure 2 shows the Arrhenius plot of conductivity for the TEGDME 0.5M LiTf solution compared to those of the IL-based electrolytes. The conductivity measured at 20°C for the TEGDME salt solution is $4.7 \cdot 10^{-4}$ Scm^{-1}, while for the electrolytes containing the IL this value is of about $3 \cdot 10^{-3}$ Scm^{-1}. Therefore, the ionic conductivity of the mixtures increased of almost one order of magnitude adding the $PYR_{1,2O1}TFSI$, in agreement with the observation of other authors[30] with negligible variations among the different compositions. All the plots of the ionic conductivity showed the same trend for the mixtures above ambient temperature. The same behaviour was reported in a previous paper,[34]

which showed an increase in conductivity for $PYR_{14}TFSI$ xLiTFSI yTEGDME mixtures with respect to both IL and TEGDME salt mixtures, with very similar ionic conductivities for the mixtures with y= 0.1 and 0.2. In our case, some differences could be observed only at lower temperature, where the $30PYR_{1,2O1}$:70TEGDME mixture showed slightly higher conductivity values.

The electrochemical stability window of the electrolytes was studied in the absence of oxygen (see Figure 3). As reported previously, the pure IL has an anodic stability superior to 4V vs. Li/Li^+ (see ref. 32). Regarding the blended electrolytes, all the mixtures showed very similar cathodic and anodic limits, and electrochemical stability windows (ESWs) wider than 5V vs Fc/Fc^+ were observed. In particular, the electrolyte decomposition was observed at potential higher than 2V vs. Fc/Fc^+ (about 4.7V vs Li/Li^+), so suggesting that the IL based mixtures are stable in the typical potential range used to charge Li-O_2 cells (below 4.5V vs Li/Li^+). At potentials more negative than -4V vs Fc/Fc^+, in parallel with Li^+ reduction an evident increase in current indicates that the reductive limit of the electrolyte has been exceeded for the studied systems.

3.3 Battery tests

Figure 4 reports the CV traces obtained for the Li-air cell containing the electrolytes mixtures. The CV of the cell containing TEGDME LiTf (Figure 4a) shows one cathodic and one anodic peak that can be attributed to the main following reactions:

$$O_2 + e^- + Li^+ \rightarrow LiO_2 \quad [1]$$

$$LiO_2 + e^- + Li^+ \rightarrow Li_2O_2 \quad [2]$$

$$LiO_2 \rightarrow O_2 + e^- + Li^+ \quad [3]$$

$$Li_2O_2 \rightarrow O_2 + 2e^- + 2Li^+ \quad [4]$$

The couples [1]-[2] and [3]-[4] taking place during ORR and OER, respectively. For the mixtures containing the IL (Figure 4b-d), at least two broad anodic peaks are instead observed. A third peak is also clearly visible for the $50PYR_{1,2O1}$:50TEGDME composition (Figure 4c), as likewise reported in the case of TEGDME and $PYR_{14}TFSI$ mixtures.[30] The CV of 0.025M LiTFSI doped O_2-saturated EMITFSI on glassy carbon electrode described by Abraham and co-workers[22] showed two anodic

peaks at about 3.2 and 3.6V versus Li^+ which were attributed to the reactions [3] and [4] respectively. Cecchetto et al.[30] for $PYR_{14}TFSI$ mixtures attributed the appearance in charge of the third peak (A1, following our scheme) to the decomposition of Li_2O, presumably formed during cell discharge, through the following reaction:

$$2Li_2O \rightarrow Li_2O_2 + 2e^- + 2Li^+ \qquad [5]$$

whereas the peaks A2 and A3 were assigned to the reactions [4] and [3], respectively. Anyway, recent DEMS studies highlighted that in dimethoxyethane (DME), as well as in heavier ethers like TEGDME, there is no evidence for formation of stable Li_2O during discharge[35-37], and Li_2O_2 is the principal product. A different description has been recently proposed to take into account the presence of distinct oxidation peaks, which is based on the formation during discharge of two electrochemical Li_2O_2 species, and namely bulk and interfacial Li_2O_2.[38] According to this description, the first oxidation peak A1 can be assigned to interfacial Li_2O_2 lying between the bulk Li_2O_2 and the carbon surface, whereas oxidation of bulk Li_2O_2 should occur at a higher potential. It can also be observed (Figure 4c) that the A3 peak seems to emerge only after three complete cycles thus likely suggesting that oxidation of bulk Li_2O_2 proceeded after that of surface Li_2O_2 and required much time to occur. By means of microelectrode voltammetry Nemanick[38] showed that the anodic peak at higher potential assigned to bulk Li_2O_2 continued to increase in total charge, similarly to what we observed here.

For the TEGDME LiTf electrolyte (Figure 4a), the anodic peak current is very high during the first cycle and then decreases during the successive ones. The opposite behaviour is observed for the IL mixtures, for which a progressive increase of the peak current is observed by increasing the cycle number. For the $30PYR_{1,2O1}$:70TEGDME mixture the cathodic peak can be clearly observed only starting from the 4^{th} cycle. In all the cases, E_{C1} is separated from E_{A1} by more than 1V, so indicating the scarce reversibility of the reaction. For all our mixtures, the CVs showed that the charge involved in the reduction process is lower than the charge involved in the oxidation one, suggesting a degradation of the electrolyte during battery recharging.

Galvanostatic cycling tests were also carried out in order to get information on the performance of the IL-based electrolytes and to study the overvoltage of ORR and OER. It has to be underlined that no catalysts were used for the fabrication of the air cathode, which was prepared by using commercial carbon black without any further treatment. The cells were cycled at increasing currents from 10 to 40 mAg_c^{-1} and were limited for the first cycles to a specific capacity of 1000 $mAhg_c^{-1}$. The results are reported for TEGDME LiTf and $50PYR_{1,2O1}$:50TEGDME in Figure 5a and 5b respectively. The TEGDME mixture (see Figure 5a) shows a very flat discharge profile at about 2.7V and a rising profile in charge, similarly to what reported by other authors,[39] delivering about 1000 $mAhg_C^{-1}$ both during the cell discharge and charge at the minimum current rate ($10mAg_C^{-1}$). The cell showed a capacity decay by increasing the current rate to $20mAg_C^{-1}$, since a value of about 200 $mAhg_c^{-1}$ was obtained for the second cycle.[17] A rather different behaviour was instead observed for the $50PYR_{1,2O1}$:50TEGDME electrolyte (see Figure 5b) that, among the tested compositions, displayed the more interesting performances. Also in this case, the first and the second discharge cycles were limited to 1000 $mAhg_C^{-1}$ but for the first discharge the cell reached the lower voltage limit of 2.2V with a maximum capacity of about 300 $mAhg_C^{-1}$, while the charge value was 1000 $mAhg_C^{-1}$. During the second cycle the current rate was doubled and, in this case, both the discharge and the charge capacity reached the maximum allowed value. Finally, for the third cycle the current was doubled again without limiting the capacity of the cell. The values of about 4000 and 2000 $mAhg_C^{-1}$ were obtained during discharge and charge, respectively, so that the Li-O_2 cell was unable to be totally recharged. After this third cycle the capacity showed a rapid decay. Recently, other authors have reported about the unusual behaviour of a cell made with a DEGDME (diethylene glycol dimethyl ether) based electrolyte,[36] which showed increasing discharge capacity values during the first 3-4 cycles and a capacity fading in the subsequent cycles. Using a pre-oxidized electrolyte, Meini et al.[36] proved in their work that the increased capacity of ether-based electrolytes upon cycling is due to electrolyte degradation. Therefore, the capacity enhancement given by combining TEGDME and the $PYR_{1,2O1}$TFSI suggests that the mixture is rather reactive in a Li-O_2 cell. This fact could be confirmed

by observing that the cathodic polarization (Figure 5b) for the highest current density ($40mAg_C^{-1}$) is lower than the cathodic polarization showed at the lower current densities, but this behaviour is not replicated in the case of the anodic polarizations. This could indicate that some different processes, for example electrolyte degradation and/or a reaction with the carbon cathode, take place in charge, thus affecting the cell capacity. Besides, Guo et al. showed that for TEGDME-based electrolytes a cut-off voltage of 4.0V led to a charge capacity lower than the discharge one and to a poor cyclability, likely due to accumulation of Li_2O_2 on cathode surface, which makes few active sites available for the following cycles.[39] In contrast, increasing the cut-off voltage to 4.5V helped in extending the battery operation. In our case, the cut-off voltage was set to 3.9V in order to prevent the carbon oxidation but, considering that the cycle performance could be dependent on the cycling procedure,[39] we cannot exclude the contribution of both electrolyte degradation and Li_2O_2 accumulation to the poor rechargeability of the cell. Also, the overvoltage for the cells containing the mixtures remained quite high and comparable to that of the cell containing the TEGDME LiTf electrolyte but, as discussed before, the air cathode needs to be optimized either by using a catalyst, or a carbon material possessing catalytic activity.

3.4 *SEM and Raman measurements on cycled air cathodes*

After the first discharge, a cell containing the $50PYR_{1,2O1}$:50TEGDME electrolyte was dismounted and the air cathode was extracted. The cathode was rinsed many times with TEGDME, dried in Ar atmosphere, and then carefully protected from exposure to air using a gas tight cell for both SEM and Raman measurements. The SEM micrographs of different portions of cathode surface are shown in Figure 6b and c compared to those of the pristine cathode (a). Bright, spherical particles emerging from the main glassy component related to the carbon black can be seen on the cathode surface. These particles can suggest the presence of Li_2O_2 as reported in other works.[23-24, 40] In order to confirm the presence of Li_2O_2 in the discharged cathode, a further investigation was performed by using micro-Raman spectroscopy. In Figure 7 we report the characteristic spectra obtained as a result of a mapping run. In the same figure the Raman spectrum from the standard Li_2O_2 powder is reported for the sake

of comparison. The spectrum reported in Figure 7a is the dominant one obtained by the mapping procedure and it is associated to the amorphous carbon material. Indeed, this is clearly demonstrated by the presence of the two broadened Raman bands peaked at about 1600 cm^{-1} and 1350 cm^{-1}, which are reminiscent of G and D modes in carbon structures.[41] The broadened and weaker features at around 500 cm^{-1} and 900 cm^{-1} are coming from glass window. The spectrum b) (associated to a small light grey region) is representative of the Raman response from 5% of the mapping area. Apart from the features at around 500 cm^{-1} and 900 cm^{-1}, the spectrum b) is completely different from the spectrum a). From the comparison with Raman spectrum from Li_2O_2 standard (Figure 7c), the presence of this oxide phase in our sample is demonstrated by the characteristic narrow modes peaked at ~ 785 and ~ 260 cm^{-1}.[42-43] No Raman peak at ~525 cm^{-1} was observed thus excluding the presence of Li_2O and confirming that Li_2O_2 is the main reaction product in ether-based cells,[35-38] whereas the additional peak at around 1090 cm^{-1} is the indication of the presence of lithium carbonate Li_2CO_3. Although ether containing electrolytes are quite stable towards superoxide radical attack, it was shown that tetraglyme-based electrolytes can decompose in cells charged up to 4.5V,[8] leading to the formation of Li_2CO_3. Besides, it was demonstrated that carbon electrodes can decompose in presence of tetraglyme-based electrolytes during charging above 3.5V, to also form Li_2CO_3.[44] Although to prevent the electrolyte and carbon decomposition the higher voltage limit was set herein to 3.9V, Li_2CO_3 detected during Raman analysis on the air cathode could be likely due to the partial decomposition of carbon and to electrolyte degradation, as also evidenced by the results of battery testing.

4. Conclusions

In this paper, we reported a thorough electrochemical characterization of IL-based electrolytes for Li-O_2 batteries. TEGDME was mixed with the ionic liquid $PYR_{1,2O1}$TFSI and LiTf salt, so obtaining electrolytes with improved conductivity and good electrochemical stability. Among the tested electrolyte compositions, the 50$PYR_{1,2O1}$:50TEGDME one showed an interesting performance in a

Li-O_2 cell, delivering about 4000 $mAhg_C^{-1}$ in discharge during the third cycle. However, the unusual behaviour of the Li-O_2 cell containing the IL-based mixture suggested electrolyte degradation during cycling. The discharged carbon electrodes were analysed by using Raman spectroscopy, and Li_2O_2 was identified on the cathode surface together with Li_2CO_3. Our investigation highlighted that carbon reactivity in presence of ILs and cycling needs to be further investigated to definitively clarify if ether-based, IL-based and their blended electrolytes are actually useful for application in Li-O_2 batteries.

Acknowledgements

This project has been financed by CARIPLO Foundation (Milano, project 2010-0506).

References

1. P.G. Bruce, S. A. Freunberger, L. J. Hardwick and J. M. Tarascon, *Nature Mat.*, **11**, 19 (2012).
2. G. Girishkumar, B. Mncloskey, A. C. Luntz, S. Swanson and W. Wilcke, *J. Phys. Chem. Lett.*, **1**, 2193 (2010).
3. D. Capsoni, M. Bini, S. Ferrari, E. Quartarone and P. Mustarelli, *J. Power Sources*, **220**, 253 (2012).
4. R. Van Noorden, *Nature*, **507**, 26 (2014).
5. M. Balaish, A. Kraytsberg and Yair Ein-Eli, *Phys.Chem.Chem.Phys.*, **16**, 2801 (2014).
6. L. J. Hardwick and P. G. Bruce, *Curr. Opinion Solid State Mater. Sci.*, **16**, 178 (2012).
7. J. Lu, L. Li, J.-B. Park, Y.-K. Sun, F. Wu and K. Amine, *Chem Rev.*, **114**, 5611 (2014).
8. S. A. Freunberger, Y. Chen, N. E. Drewett, L. J. Hardwick, F. Bardé and P. G. Bruce, *Angew. Chem. Int. Ed.*, **50**, 8609 (2011).
9. B. D. McCloskey, D. S. Bethune, R. M. Shelby, G. Girishkumar. A. C. Luntz, *J. Phys. Chem. Lett.*, **2**, 1161 (2011).
10. V. S. Bryantsev, V. Giordani, W. Walker, M. Blanco, S. Zecevic K. Sasaki, J. Uddin, D. Addison and G. V. Chase, *J. Phys. Chem. A*, **115**, 12399 (2011).
11. V. S. Bryantsev, J. Uddin, V. Giordani, W. Walker, D. Addison and G. V. Chase, *J. Electrochem. Soc.*, **160**, A160 (2013).
12. Y. Chen, S. A. Freunberger, Z. Peng, F. Bardé and P. G. Bruce, *J. Am. Chem. Soc.*, **134**, 7952 (2012).
13. V. Giordani, V. S. Bryantsev, J. Uddin, W. Walker, G. V.Chase and D. Addison, *ECS Electrochem. Let.*, **3**, A11 (2014).
14. C. O. Laoire, S. Mukerjee, E. J. Plichta and M. A. Hendrickson, *J. Phys. Chem. C*, **114**, 9178 (2010).

15. D. Xu, Z.-L. Wang, J.-J. Xu, L.-L. Zhang and X.-B. Zhang, *Chem. Commun.* **48**, 6948 (2012).
16. H.-G. Jung, J. Hassoun, J.-B. Park, Y.-K. Sun and B. Scrosati, *Nat. Chem*, **4**, 579 (2012).
17. C. O Laoire, S. Mukerjee, E. J. Plichta, M. A. Hendrickson and K. M. Abraham, *J. Electrochem. Soc.*, **158**, A302 (2011).
18. M. Marinaro, S. Theil, L. Joerissen and M. Wohlfahrt-Mehrens, *Electrochimica Acta*, **108**, 795 (2013).
19. K. Xie and H. Wang, *Electrochimica Acta*, **64**, 19 (2012).
20. T. Kuboki, T. Okuyama, T. Ohsaki and N. Takami, *J. Power Sources*, **146**, 766 (2005).
21. S. Monaco, F. Soavi and M. Mastragostino, *J. Phys. Chem. Lett.*, **4**, 1379 (2013).
22. C. J. Allen, S. Mukerjee, E. J. Plichta, M. A. Hendrickson and K. M. Abraham, *J. Phys. Chem. Lett.*, **2**, 2420 (2011).
23. F. Soavi, S. Monaco and M. Mastragostino, *J. Power Sources*, **224**, 115 (2013).
24. J. Zeng, J. R. Nair, C. Francia, S. Bodoardo and N. Penazzi, *Int. J. Electrochem. Sci.*, **8**, 3912 (2013).
25. C. J. Allen, J. Hwang, R. Kautz, S. Mukerjee, E. J. Plichta, M. A. Hendrickson and K. M. Abraham, *J. Phys. Chem. C*, **116**, 20755 (2012).
26. H. Nakamoto, Y. Suzuki, T. Shiotsuki, F. Mizuno, S. Higashi, K. Takechi, T. Asaoka, H. Nushikoori and H. Iba, *J. Power Sources*, **243**, 19 (2013).
27. J. Reiter, E. Paillard, L. Grande, M. Winter, S. Passerini, *Electrochimica Acta*, **91**, 101 (2013).
28. T. Zhang and H. Zhou, *Nat. Comm*, **4**, 1817 (2013).
29. T. Zhang and H. Zhou, *Angew. Chem. Int. Ed.*, **51**, 11062 (2012).
30. L. Cecchetto, M. Salomon, B. Scrosati and F. Croce, *J. Power Sources*, **213**, 233 (2012).
31. B. G. Kim, J.-N. Lee, D. J. Lee, J.-K. Park and J. W. Choi, *ChemSusChem*, **6**, 443 (2013).

32. S. Ferrari, E. Quartarone, P. Mustarelli, A. Magistris, S. Protti, S. Lazzaroni, M. Fagnoni and A. Albini, *J. Power Sources*, **194**, 45 (2009).
33. P. C. Howlett, E. I. Izgorodina, M. Forsyth, D. R. MacFarlane, *Z. Phys. Chem.*, **220**, 1483 (2006).
34. J. H. Shin and E. J. Cairns, *J. Electrochem. Soc.*, **155**, A368 (2008).
35. B. D. McCloskey, R. Scheffler, A. Speidel, G. Girishkumar and A. C. Luntz *J. Phys. Chem. C*, **116**, 23897 (2012).
36. S. Meini, M. Piana, H. Beyer, J. Schwammlein and H. A. Gasteiger, *J. Electrochem. Soc.*, **159**, A2135 (2012).
37. N. Tsiouvaras, S. Meini, I. Buchberger and H. A. Gasteiger, *J. Electrochem. Soc.*, **160**, A471 (2013).
38. E. J. Nemanick, *J. Power Sources*, **247**, 26 (2014)
39. X. Guo and N. Zhao, *Adv. Energy Materials*, **3**, 1413 (2013).
40. B. D. Adams, C. Radtke, R. Black, M. L. Trudeau, K. Zaghib and L. F. Nazar, *Energy Environ. Sci.*, **6**, 1772 (2013).
41. D. Ravelli, S. Montanaro, C. Tomasi, P. Galinetto, E. Quartarone, D. Merli, P. Mustarelli and M. Fagnoni, *ChemPlusChem*, **1**, 210 (2012).
42. G. M. Veith, N. J. Dudney, J. Howe and J. Nanda, *J. Phys. Chem. C*, **115**, 14325 (2011).
43. S. Higashi, Y. Kato, K. Takechi, H. Nakamoto, F. Mizuno, H. Nishikoori, H. Iba and T. Asaoka, *J. Power Sources*, **240**, 14 (2013).
44. M. M. Ottakam Thotiyl, S. A. Freunberger, Z. Peng and P. G. Bruce, *J. Am. Chem. Soc.*, **135**, 494 (2013).

Figure captions

Figure 1- a) TGA and b) DSC traces of the mixtures compared to TEGDME LiTf.

Figure 2- Ionic conductivity plots as a function of the temperature for the $xPYR_{1,2O1}$:(x-1)TEGDME electrolytes. The conductivity of the TEGDME-LiTf 0.5M and of the pure IL is also reported as a comparison. The lines are only guides for eyes.

Figure 3- Linear sweep voltammetry in Ar for the IL based electrolytes and TEGDME-LiTf.

Figure 4- Cyclic voltammetry performed on Li-air cells containing a) TEGDME LiTf 0.5M, b) $30PYR_{1,2O1}$:70TEGDME, c) $50PYR_{1,2O1}$:50TEGDME and d) $70PYR_{1,2O1}$:30TEGDME electrolytes (scan rate $0.1mVsec^{-1}$, 2.4-4.2V potential range).

Figure 5- Discharge and charge capacity per carbon weight vs. cell potential for: a) TEGDME LiTf 0.5M and b) $50PYR_{1,2O1}$:50TEGDME electrolytes.

Figure 6- SEM micrographs of: a) pristine cathode, and (b, c) different portions of the cathode after first discharge of a cell containing the $50PYR_{1,2O1}$:50TEGDME electrolyte.

Figure 7 -Representative Raman spectra at room temperature resulting from a mapping run on a sample region 10x10 μm for the air cathode shown in Fig 6b and c. a) Spectrum from black coloured region, b) spectrum from light grey region and c) spectrum from standard Li_2O_2.

Figure

Figure 1

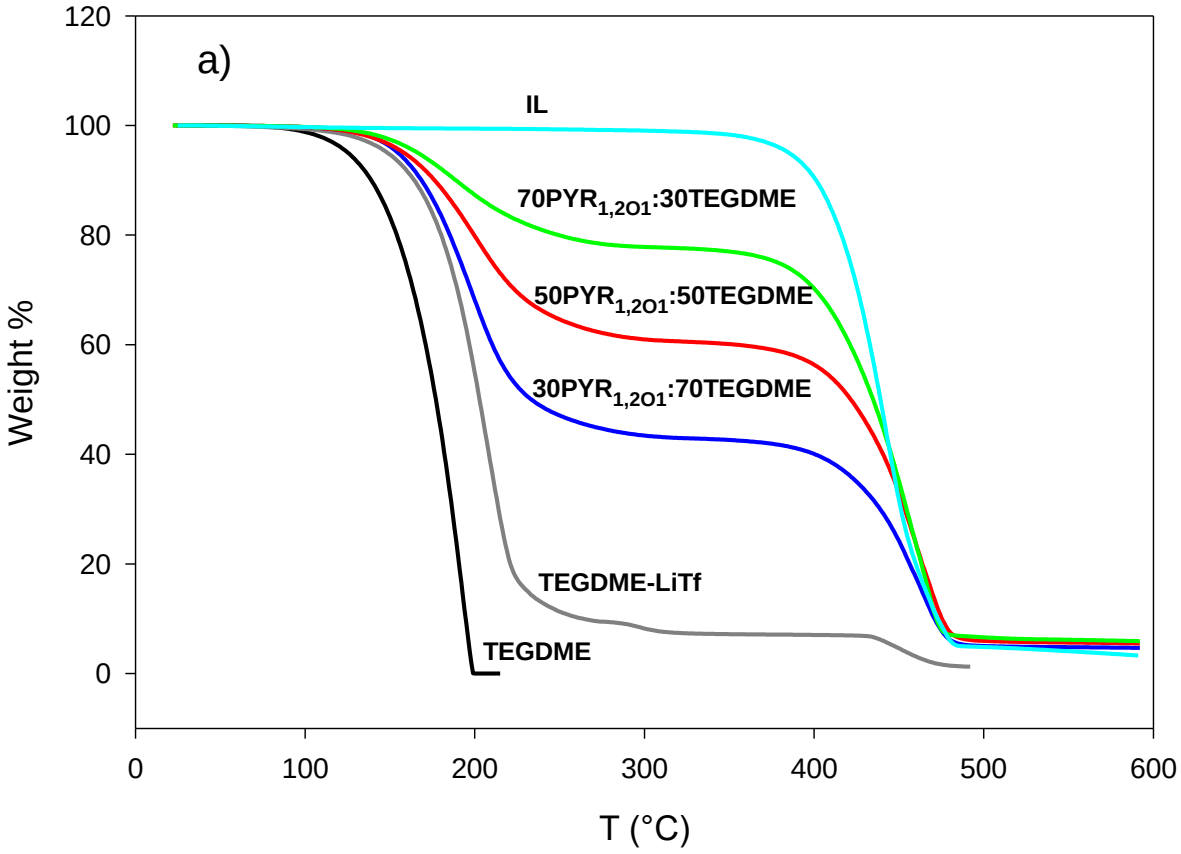

Figure 1

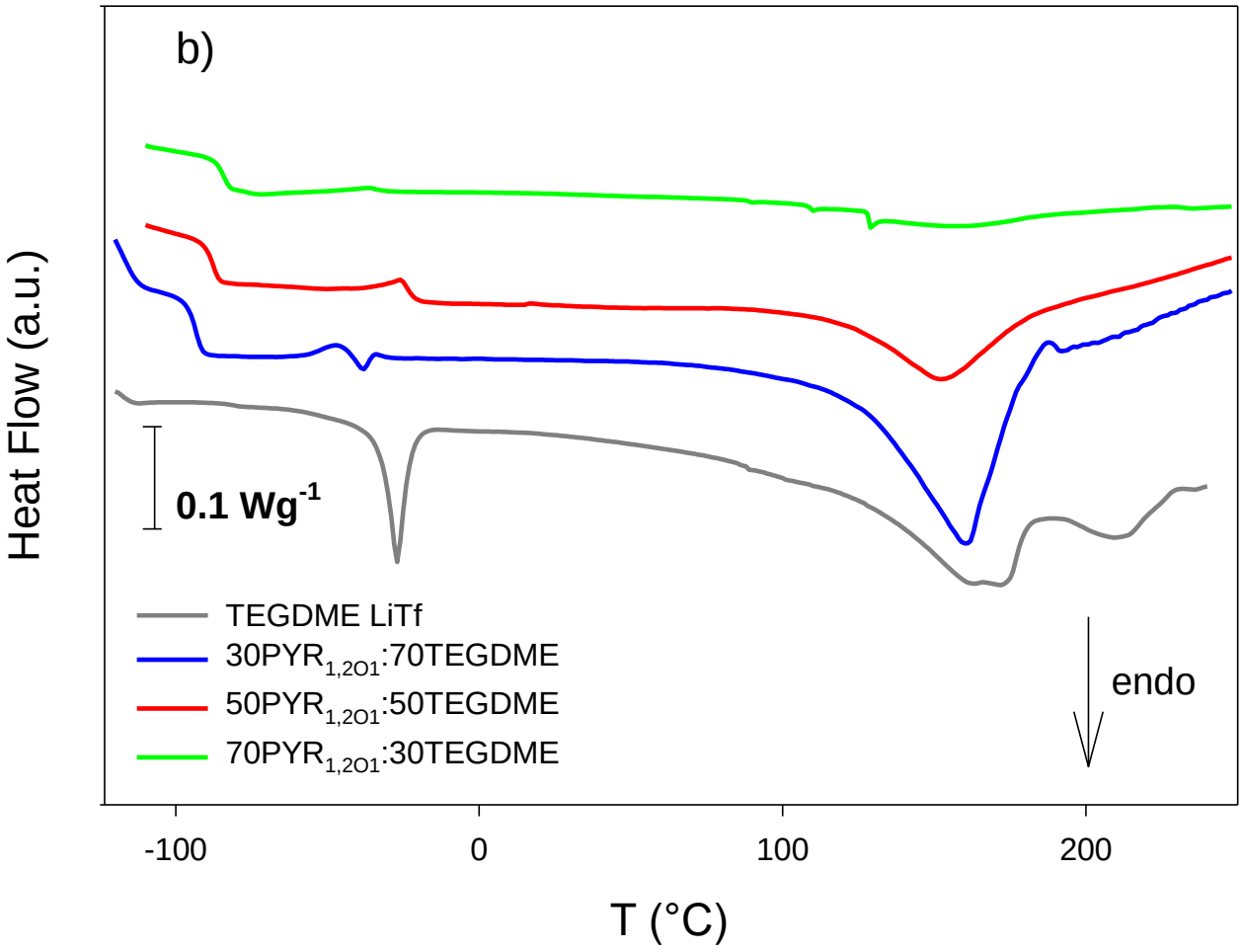
b)
Heat Flow (a.u.)
0.1 Wg-1
TEGDME LiTf
30PYR1,2O1:70TEGDME
50PYR1,2O1:50TEGDME
70PYR1,2O1:30TEGDME
endo
-100
0
100
200
T (°C)

Figure 2

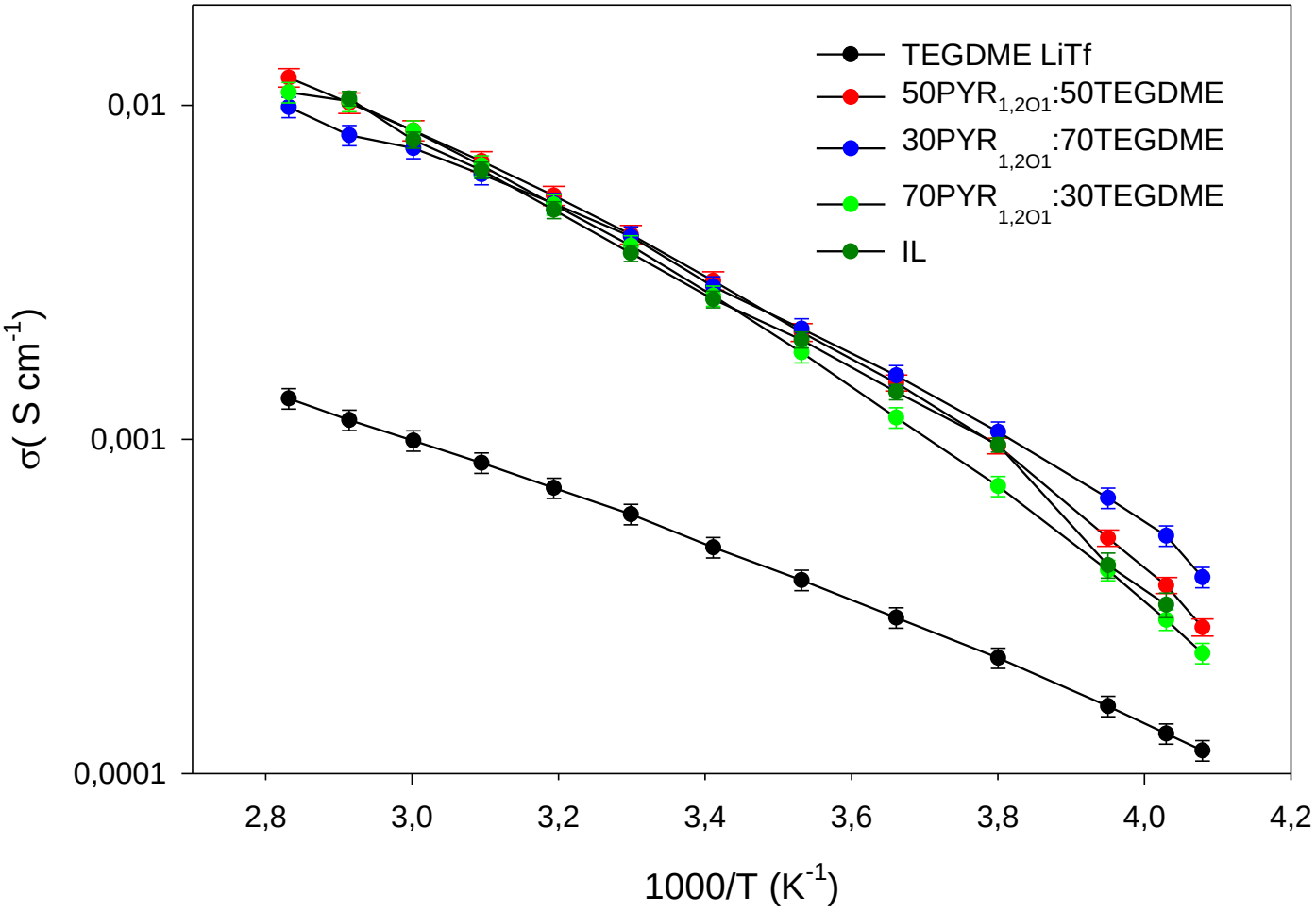
TEGDME LiTf
50PYR1,2O1:50TEGDME
30PYR1,2O1:70TEGDME
70PYR1,2O1:30TEGDME
IL
0,01
0,001
0,0001
σ(S cm-1)
2,8
3,0
3,2
3,4
3,6
3,8
4,0
4,2
1000/T (K-1)

Figure 3

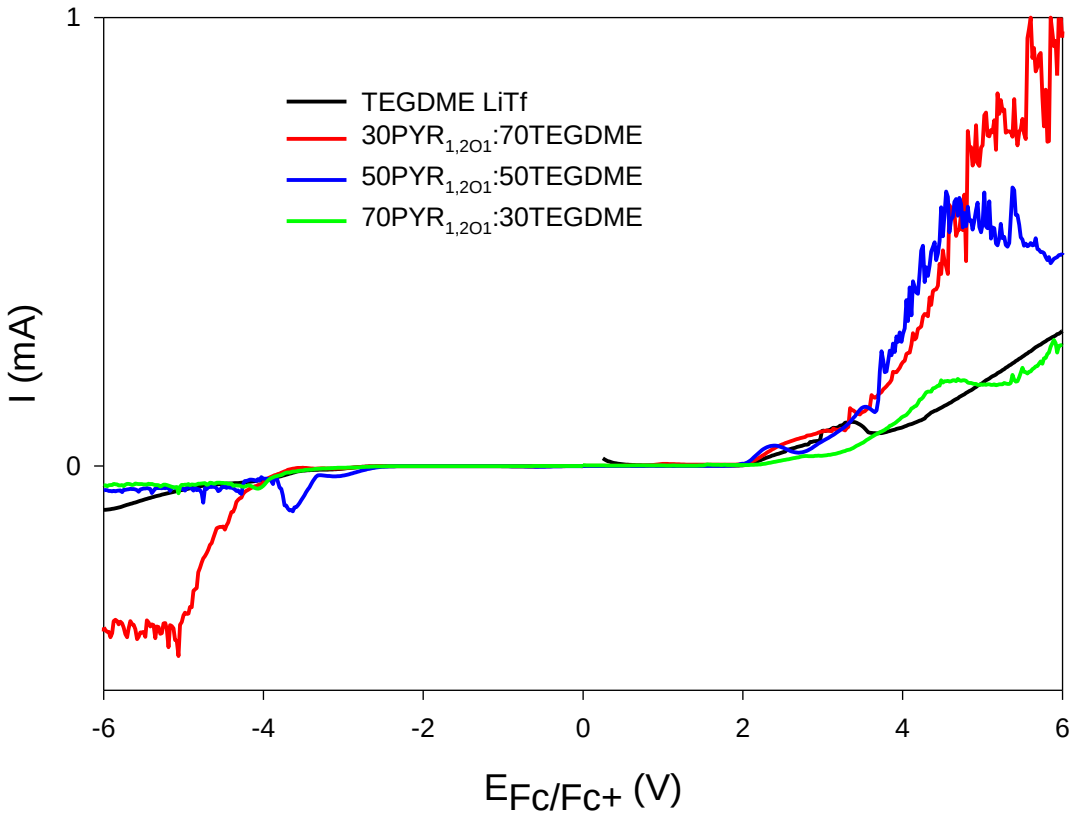
1
0
I (mA)
TEGDME LiTf
30PYR1,2O1:70TEGDME
50PYR1,2O1:50TEGDME
70PYR1,2O1:30TEGDME
-6
-4
-2
0
2
4
6
EFc/Fc+ (V)

Figure 4

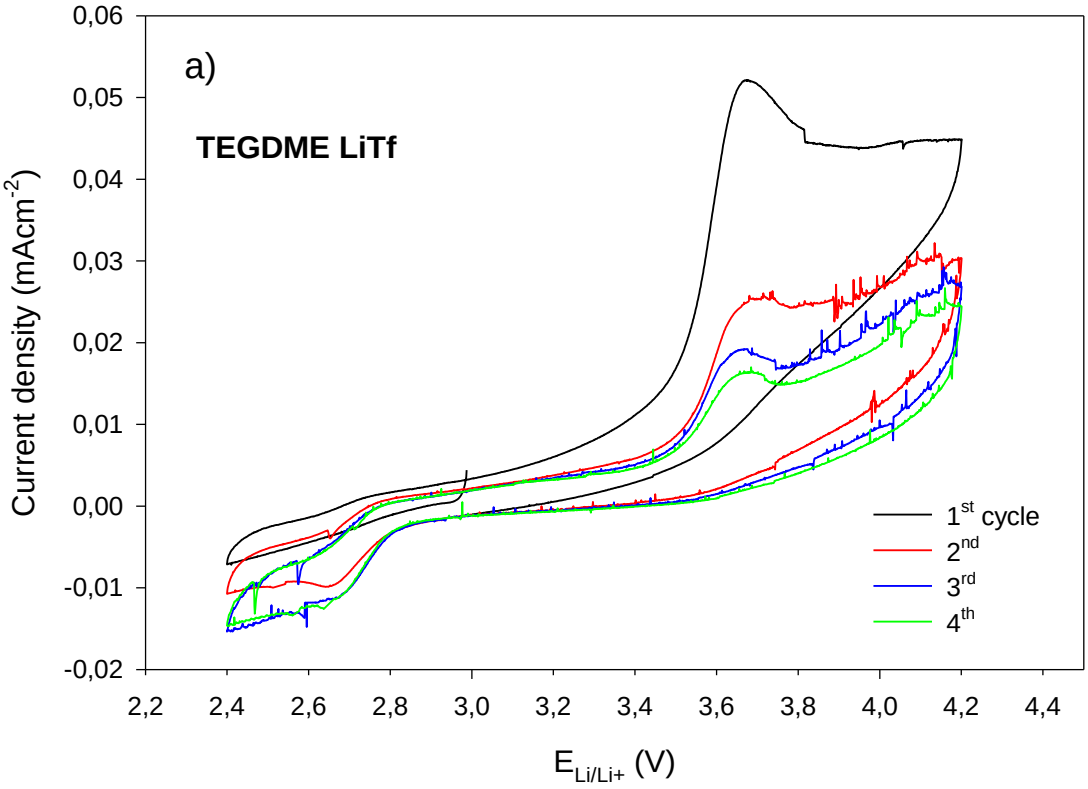
a)
TEGDME LiTf
Current density (mAcm-2)
0,06
0,05
0,04
0,03
0,02
0,01
0,00
-0,01
-0,02
2,2
2,4
2,6
2,8
3,0
3,2
3,4
3,6
3,8
4,0
4,2
4,4
E Li/Li+ (V)
1st cycle
2nd
3rd
4th

Figure 4

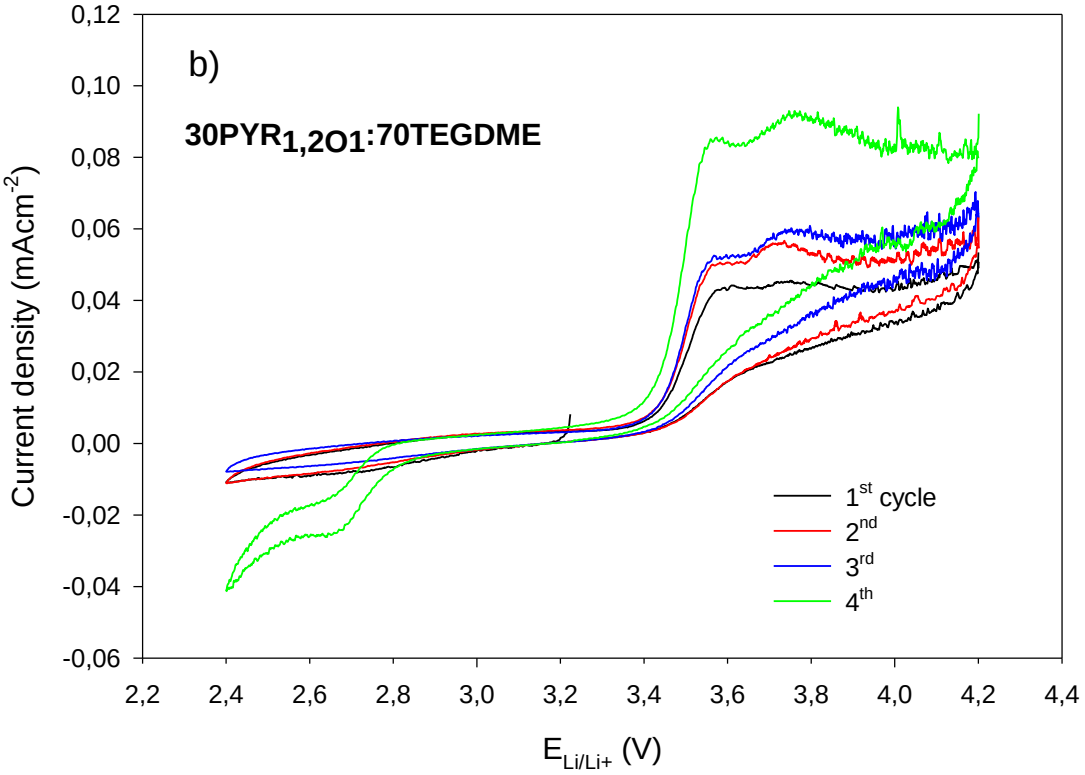
b)
30PYR1,2O1:70TEGDME
Current density (mAcm-2)
0,12
0,10
0,08
0,06
0,04
0,02
0,00
-0,02
-0,04
-0,06
2,2
2,4
2,6
2,8
3,0
3,2
3,4
3,6
3,8
4,0
4,2
4,4
ELi/Li+ (V)
1st cycle
2nd
3rd
4th

Figure 4

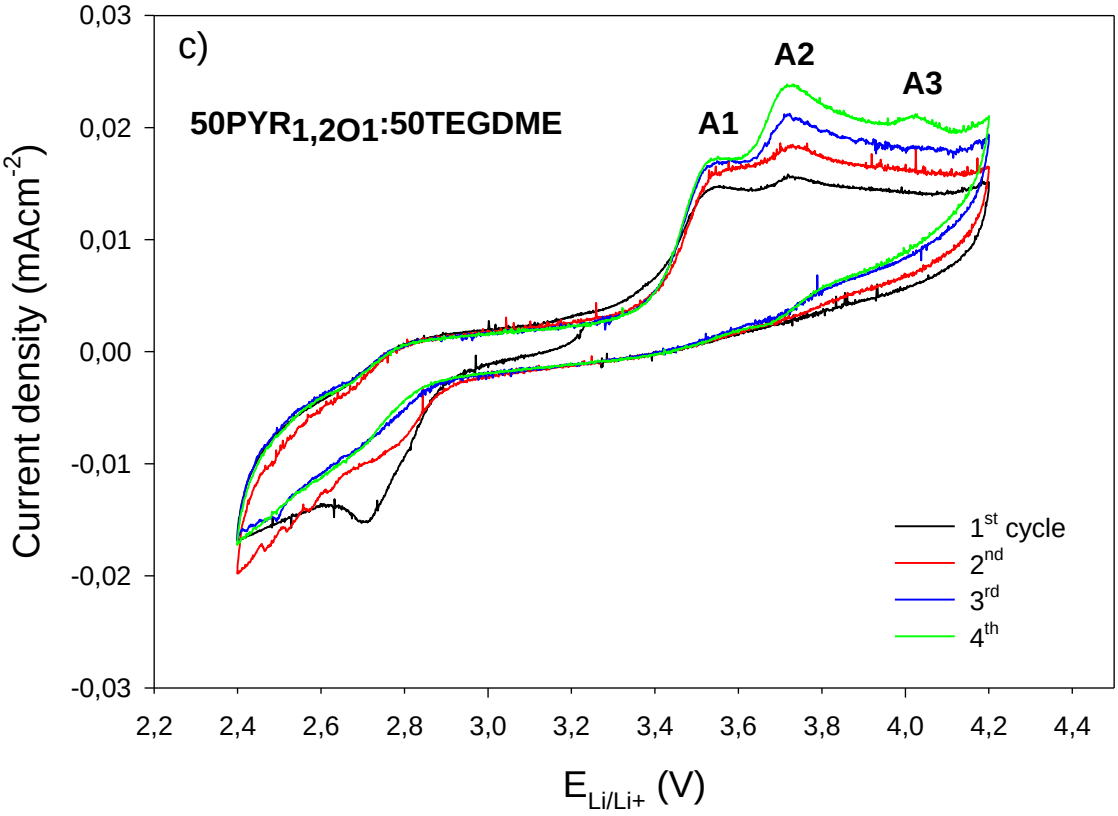
c)
50PYR1,2O1:50TEGDME
A1
A2
A3
1st cycle
2nd
3rd
4th
Current density (mAcm-2)
ELi/Li+ (V)
0,03
0,02
0,01
0,00
-0,01
-0,02
-0,03
2,2
2,4
2,6
2,8
3,0
3,2
3,4
3,6
3,8
4,0
4,2
4,4

Figure 4

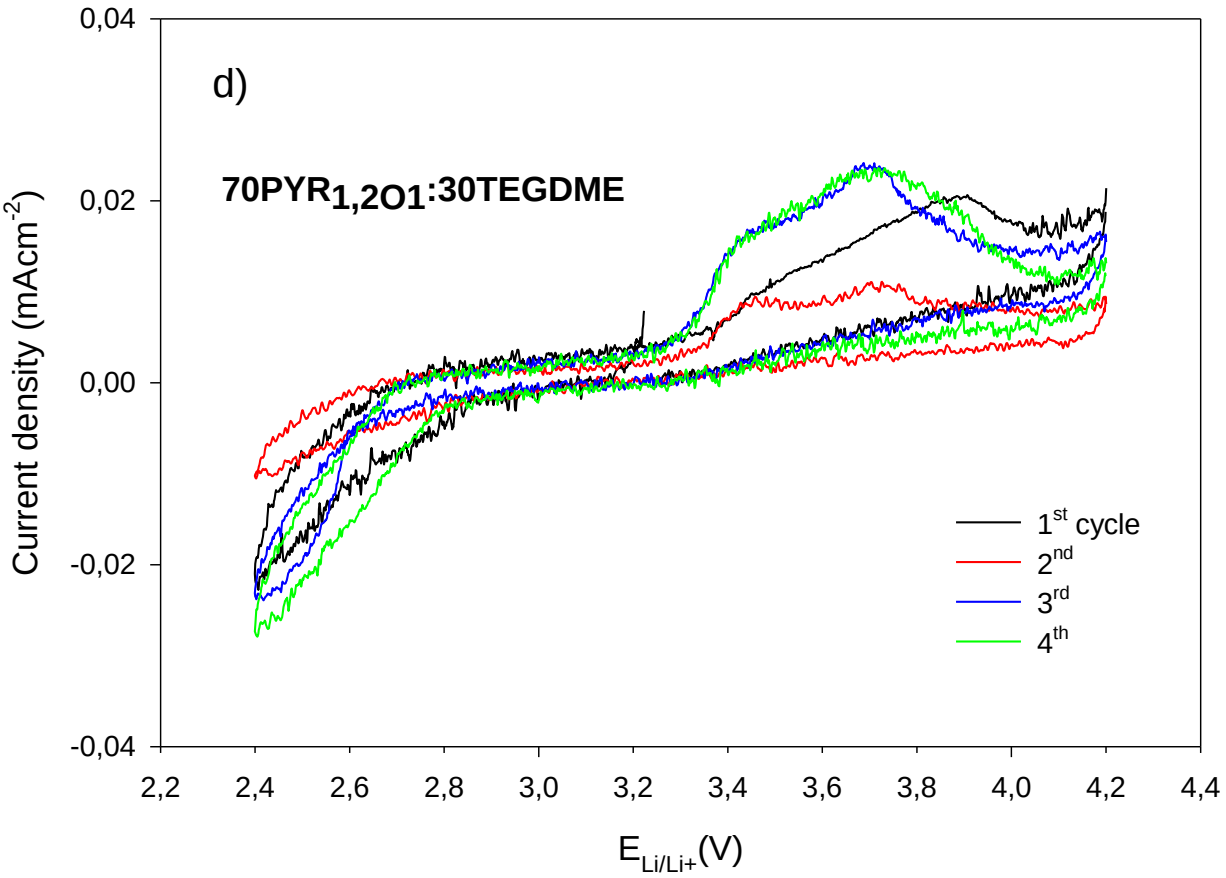
d)
70PYR1,2O1:30TEGDME
Current density (mAcm-2)
0,04
0,02
0,00
-0,02
-0,04
2,2
2,4
2,6
2,8
3,0
3,2
3,4
3,6
3,8
4,0
4,2
4,4
ELi/Li+(V)
1st cycle
2nd
3rd
4th

Figure 5

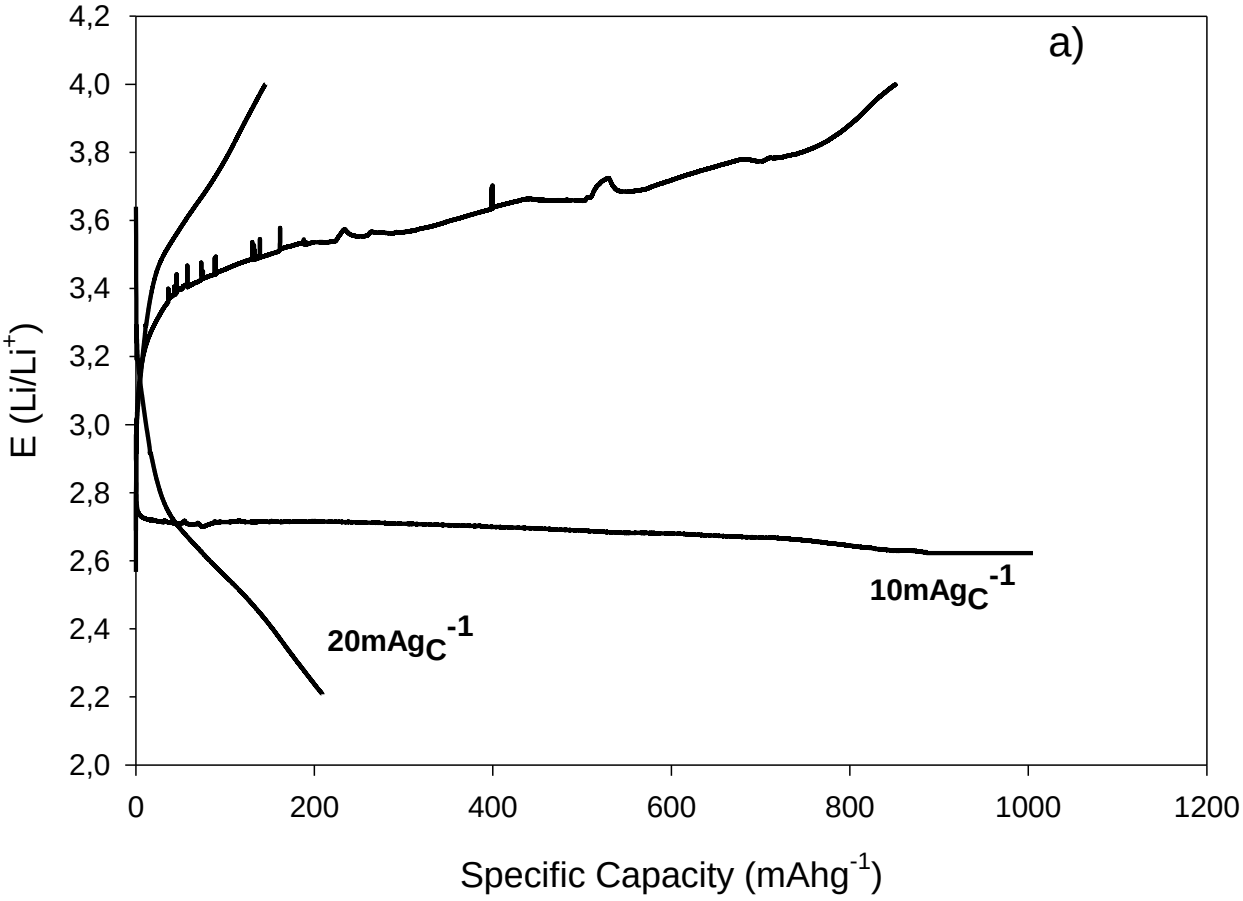
a)
4,2
4,0
3,8
3,6
3,4
3,2
3,0
2,8
2,6
2,4
2,2
2,0
E (Li/Li+)
0
200
400
600
800
1000
1200
Specific Capacity (mAhg-1)
10mAgC-1
20mAgC-1

Figure 5

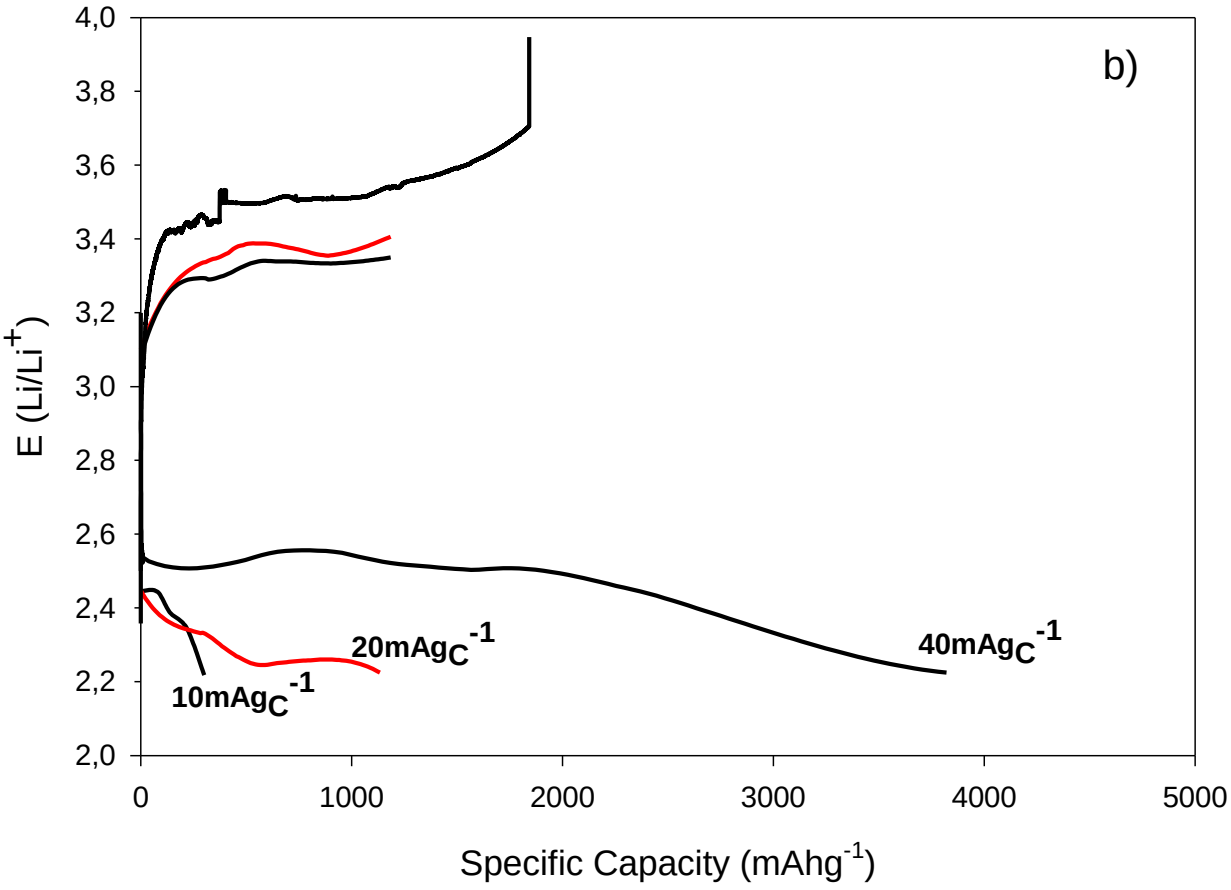
b)
E (Li/Li+)
4,0
3,8
3,6
3,4
3,2
3,0
2,8
2,6
2,4
2,2
2,0
0
1000
2000
3000
4000
5000
Specific Capacity (mAhg-1)
10mAgC-1
20mAgC-1
40mAgC-1

Figure 6

a)

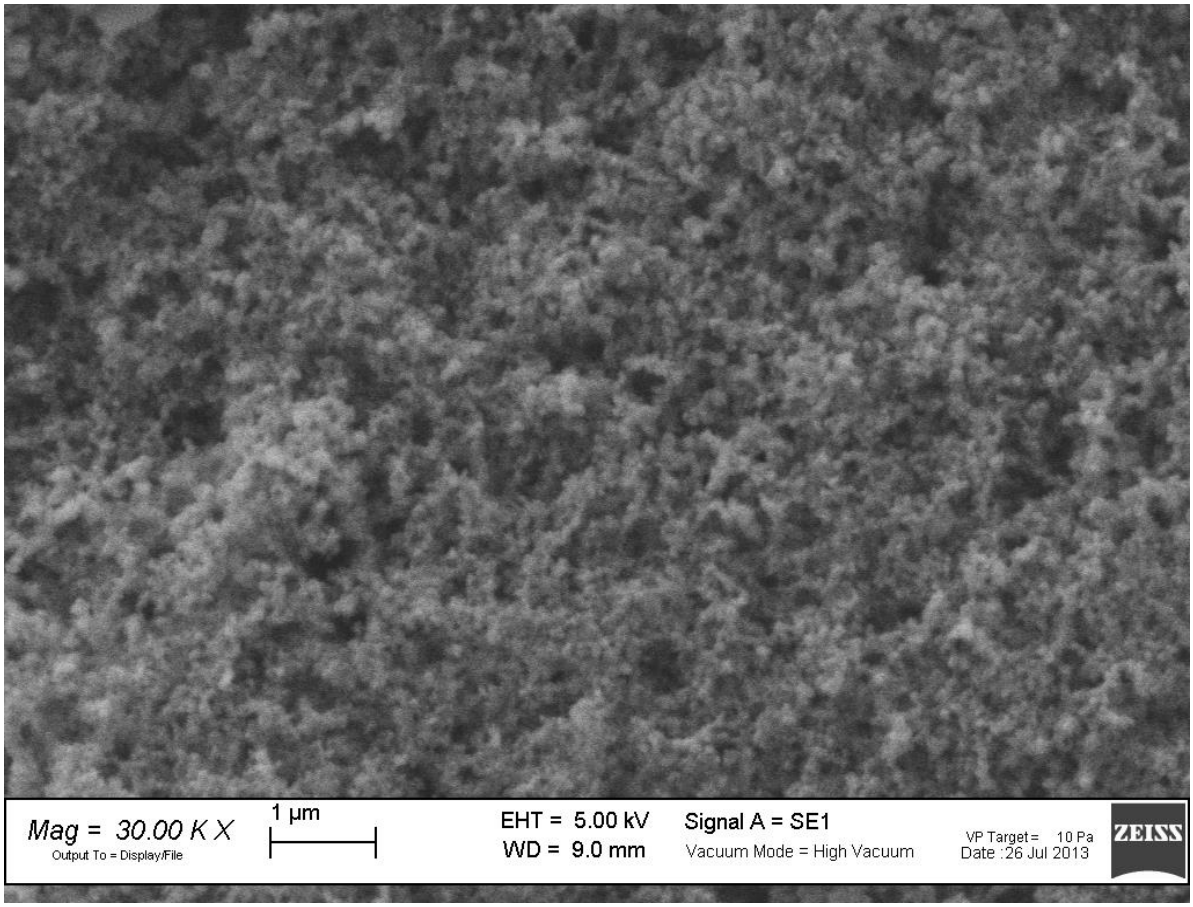
Mag = 30.00 K X
Output To = Display/File
1 µm
EHT = 5.00 kV
WD = 9.0 mm
Signal A = SE1
Vacuum Mode = High Vacuum
VP Target = 10 Pa
Date :26 Jul 2013
ZEISS

b)

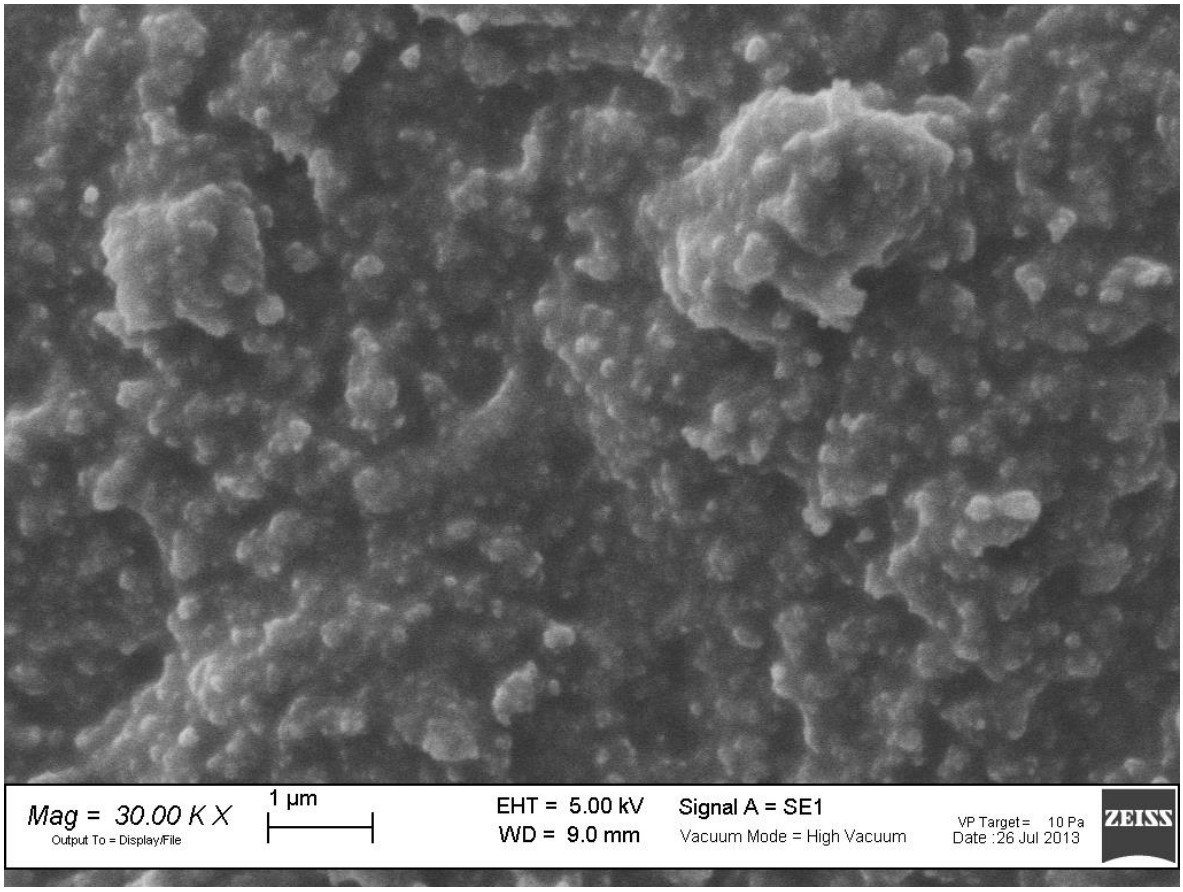
Mag = 30.00 K X
Output To = Display/File
1 µm
EHT = 5.00 kV
WD = 9.0 mm
Signal A = SE1
Vacuum Mode = High Vacuum
VP Target = 10 Pa
Date :26 Jul 2013
ZEISS

c)

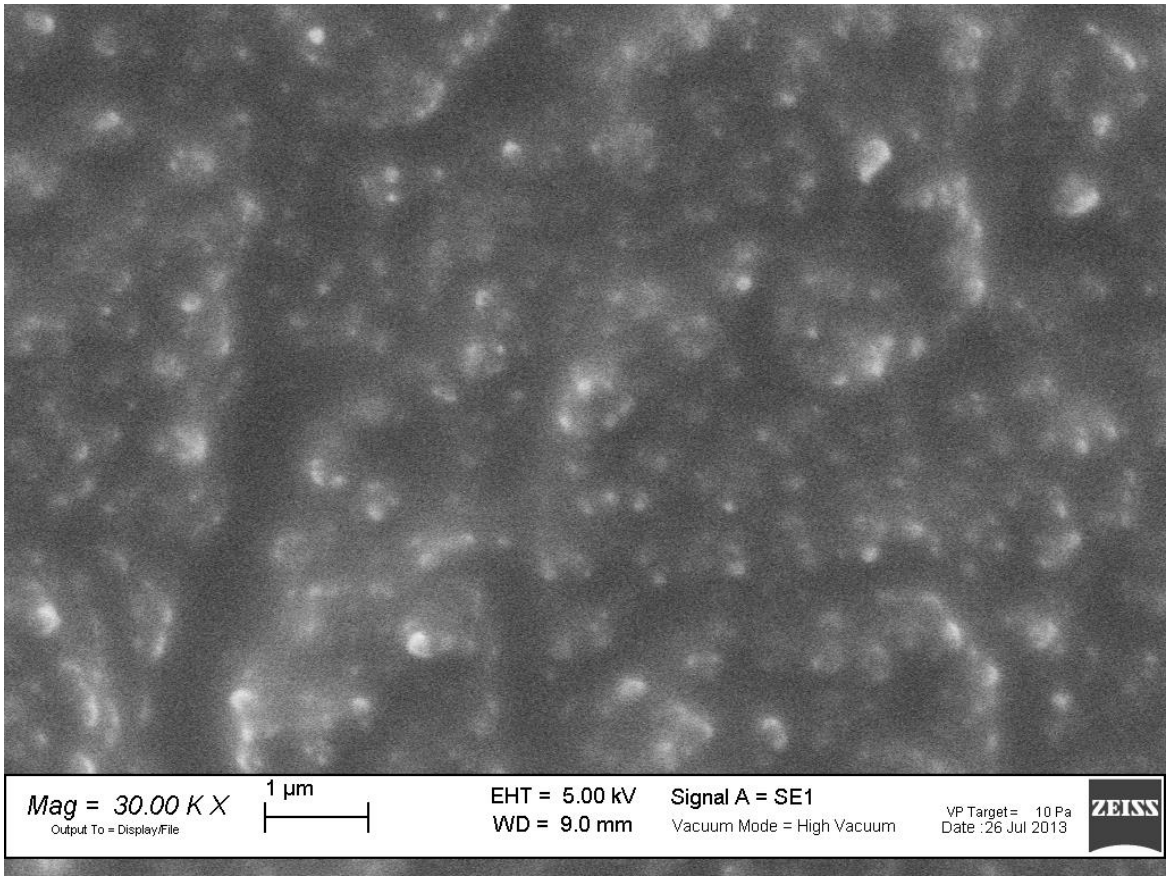
Mag = 30.00 K X
Output To = Display/File
1 µm
EHT = 5.00 kV
WD = 9.0 mm
Signal A = SE1
Vacuum Mode = High Vacuum
VP Target = 10 Pa
Date :26 Jul 2013
ZEISS

Figure 7

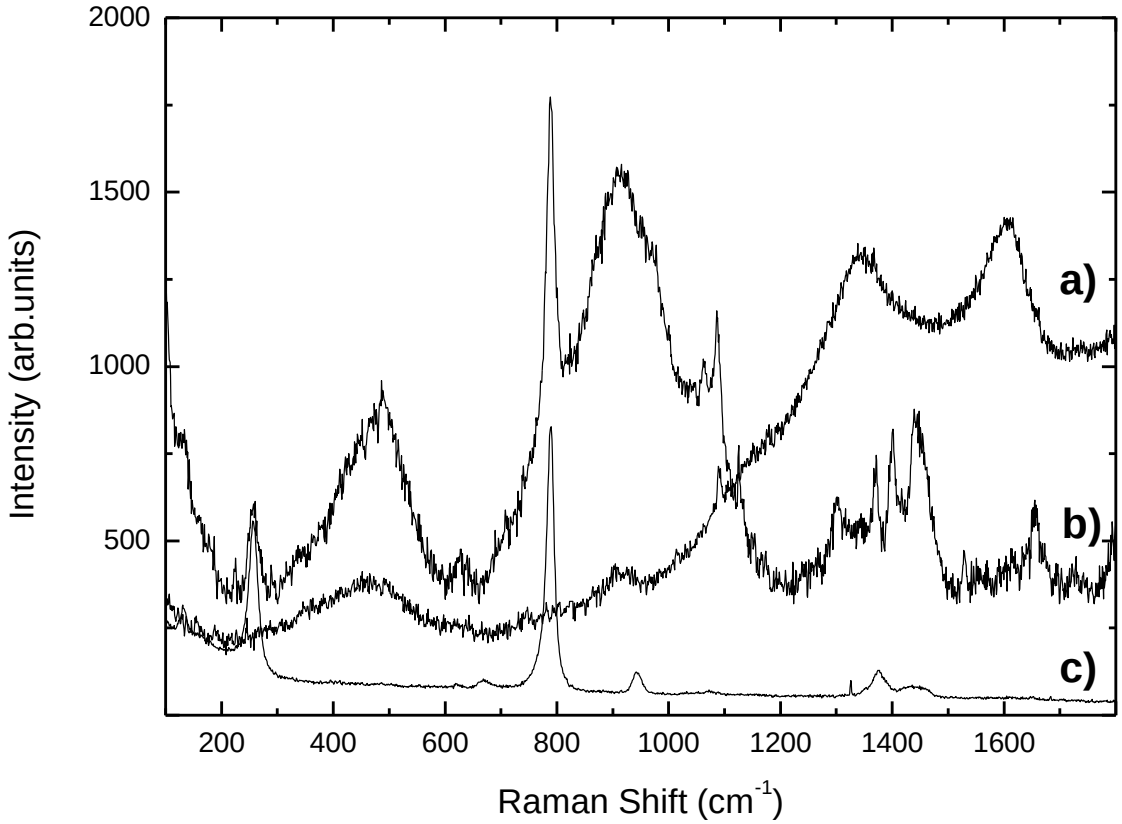
2000
1500
1000
500
Intensity (arb.units)
200
400
600
800
1000
1200
1400
1600
Raman Shift (cm-1)
a)
b)
c)